Continuous-wave tunable and femtosecond mode-locked laser operation of Yb:$NaY(MoO_4)_2$

Andreas Schmidt,[1] Simon Rivier,[1] Valentin Petrov,[1] Uwe Griebner,[1,*] Xiumei Han,[2] José María Cano-Torres,[2] Alberto García-Cortés,[2] María Dolores Serrano,[2] Concepción Cascales,[2] and Carlos Zaldo[2]

[1]*Max Born Institute for Nonlinear Optics and Ultrafast Spectroscopy, 2A Max-Born-Strasse, D-12489 Berlin, Germany*

[2]*Instituto de Ciencia de Materiales de Madrid, Consejo Superior de Investigaciones Científicas, c/ Sor Juana Inés de la Cruz 3, Cantoblanco, E-28049 Madrid, Spain*

**Corresponding author: griebner@mbi-berlin.de*

Received May 1, 2008; revised June 17, 2008; accepted June 17, 2008; posted June 23, 2008 (Doc. ID 95660); published July 29, 2008

Continuous-wave and mode-locked laser operations of Yb^{3+} in the disordered flux-grown $NaY(MoO_4)_2$ are demonstrated. The maximum slope efficiency achieved with Ti:sapphire and diode laser pumping is 63% and 38.6%, respectively. The continuous-wave tunability extends from 1005 to 1059 nm, and laser pulses with a duration of 91 fs at 1026 nm are obtained at a repetition rate of 90 MHz and an average power of 20 mW under Ti:sapphire laser pumping. Yb^{3+}-doped $NaY(MoO_4)_2$ is locally disordered and exhibits the largest absorption and emission cross sections known so far for tetragonal double tungstates or molybdates.

OCIS codes: 140.5680, 140.3070, 160.5690.

1. INTRODUCTION

Laser tunability and ultrashort (fs) pulsed laser operation require active ions with broad optical bandwidths. Since the 4*f* electrons of trivalent lanthanides are shielded from the crystal host field by outer 5*s* and 5*p* electrons, their spectral lines are relatively narrow. However, due to the presence of two sites occupied quasi-randomly by monovalent or trivalent cations, the tetragonal (space group $I\bar{4}$) double tungstate (DT) and double molybdate (DM) crystal hosts with formula $MT(XO_4)_2$ (*MTX* for short), where *M* is a monovalent alkali metal (most often Li^+ or Na^+), *T* is an optically passive trivalent cation, $T=Bi^{3+}$, Y^{3+}, La^{3+}, Gd^{3+}, or Lu^{3+}, and $X=W^{6+}$ or Mo^{6+} exhibit broader optical bands of the optically active lanthanide dopants than those observed in their monoclinic counterparts with $M=K^+$, which have a single site for each cation.

In the last few years a systematic search for the most suitable tetragonal DT or DM crystal host for ultrafast Yb^{3+} lasers has been undertaken. Tunable continuous-wave (cw), *Q*-switched, and mode-locked laser operation have been previously achieved in several of these crystals including Yb:Na*T*W, *T*=Y [1–3], La [4,5], Gd [6,7], or Lu [8], Yb:LiGdMo [9], and Yb:NaLaMo [4,10,11]. In the DT series the largest cross sections and shortest pulses (53 fs) were achieved in Yb:NaYW [1]. Multiwatt cw emission has been obtained under laser diode pumping either up to 5.2 W in Yb:NaYW using a simple two mirror cavity [2] or up to 16.5 W in Yb:NaGdW using a thin-disk geometry with improved heat management [12]. Large single crystals of Na*T*W, *T*=Y, La, and Gd can be obtained by the Czochralski (Cz) growth method, although high temperatures (1200 °C–1260 °C) are required, and the crystals obtained are slightly deficient in Na. This deficiency is compensated by extra incorporation of trivalent cations. The top seeded solution growth (TSSG) method using $Na_2W_2O_7$ or Na_2WO_4 fluxes has to be used to grow NaLuW because it melts with decomposition, but it has also been applied to avoid the Na losses during the growth of other Na*T*W (*T*=Y, La, and Gd) crystals [13].

Isostructural DM crystals have lower melting temperatures (1128 °C, 1140 °C, and 1182 °C for Na*T*Mo, *T*=*Y*, La, and Gd, respectively) that *a priori* is expected to simplify their crystal growth. Moreover, the absorption cross sections (σ_{ABS}) reported are larger for the molybdates, e.g., $\sigma_{ABS}(977\ \text{nm})=2.2-2.5\times10^{-20}\ \text{cm}^2$ for the π-spectrum of Yb:NaLaMo [10,14] while $\sigma_{ABS}(977\ \text{nm})=1.6\times10^{-20}\ \text{cm}^2$ for the π-spectrum of Yb:NaLaW [5]. However, the laser operation is scarcely studied in such molybdate crystals. In fact lasing was demonstrated only with Yb:NaLaMo of the Na*T*Mo series, both under Ti:sapphire [4,11] and diode laser [10,11] pumping, but in all cases the slope efficiencies obtained were modest, $\eta<40\%$. Using Yb:LiGdMo higher slope efficiencies up to 64.5% were demonstrated [9].

Yb:NaYMo seems a promising crystal for laser applications since it melts congruently, and the Cz method has been applied to pull large crystals; the similar ionic radii of Yb^{3+} and Y^{3+} are expected to lead to a segregation coefficient for Yb close to unity and good crystal uniformity; σ_{ABS} values larger than in isostructural DT have been recently reported, i.e., $\sigma_{ABS}(976\ \text{nm})=3.2\times10^{-20}$ and $2.49\times10^{-20}\ \text{cm}^2$ for the π- and σ-spectra of Yb:NaYMo, respectively [15]. However, crystals pulled by the Cz method systematically appear colored due to a broad optical absorption (OA) covering the whole visible region (from 800 nm to the crystal bandgap) [15–18]. Although this coloration has been partially removed by several days of annealing at 850 °C–900 °C in air or oxygen atmo-

sphere, the influence of the remaining defects on the laser properties is yet unknown.

In this paper we present the room temperature and 6 K spectroscopic characteristics of Yb:NaYMo crystals grown by two different methods, Cz and TSSG, and demonstrate for the first time to our knowledge efficient cw laser operation at 300 K under Ti:sapphire and diode laser pumping and in the mode-locked regime.

2. CRYSTAL GROWTH AND OPTICAL CHARACTERIZATION

Yb-doped NaYMo crystals were grown in air by the Cz method using pulling equipment with the crystal diameter control described previously [19]. The starting materials were analytical-grade Alfa Aesar 99.99% Y_2O_3, 99.9% Yb_2O_3, 99.5% Na_2CO_3, and 99.95% MoO_3. Undoped a-cut oriented NaYW seeds were used. The synthesized materials were melted in a Pt crucible at a temperature 30 °C higher than the melting point and homogenized for 3 h. The optimum crystallization temperature was determined by monitoring the crucible weight changes during seeding. The rotation rate was 20 rpm, and the pulling rate was 2 mm/h for the crystal with 1 at. % concentration of Yb in the melt and 1.2 mm/h for crystals with high concentration, i.e., 10 at. % Yb in the melt. The grown crystals were cooled down to room temperature at a rate of 10 °C/h. The crystal dimensions were 35 mm in diameter and 40 mm in length. The as-grown crystals were colored [see Fig. 1(a)]. This coloration is due to a broad absorption peaking at about 550 nm (see Fig. 2). The visual coloration was removed by the annealing of plates with a thickness of less than 3 mm in air at 900 °C for up to 72 h [see Fig. 1(b)]. In this way a uniform transparency was achieved. After annealing the sample surface was covered by a white layer that was removed by polishing. The annealing helps to suppress the broad band at 550 nm, but still residual absorption is observed starting from 800 nm and increasing toward the crystal bandgap.

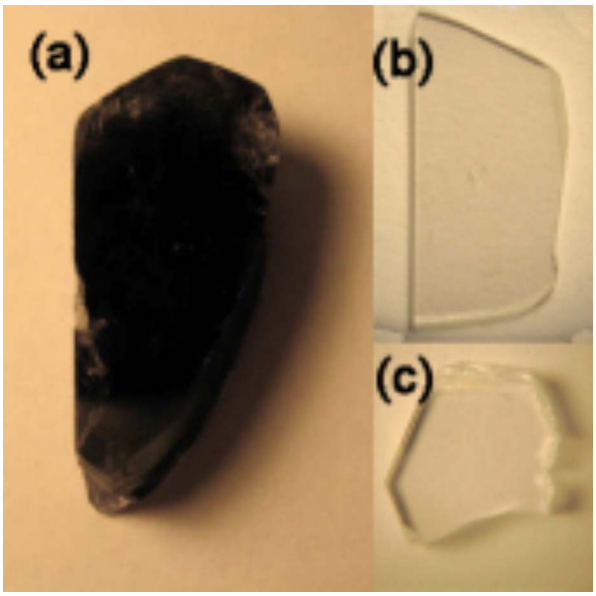

Fig. 1. (Color online) (a) Yb:NaYMo sample as-grown by the Cz method. (b) Yb:NaYMo sample grown by the Cz method after annealing at 900 °C for 72 h. (c) Yb:NaYMo sample as-grown by the TSSG method.

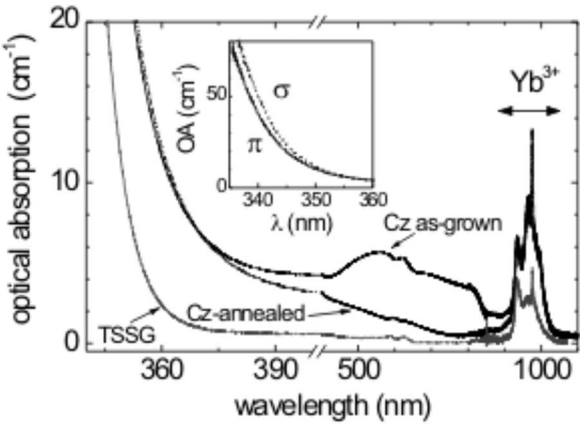

Fig. 2. Comparison of the room temperature unpolarized OA of as-grown and annealed (for 72 h at 900 °C) 8.4 at. % Yb:NaYMo Cz-grown crystals with that of a 3.3 at. % Yb:NaYMo TSSG crystal. The inset shows the room temperature polarized OA near the NaYMo bandgap for a TSSG sample.

The TSSG method without pulling was also used to grow Yb:NaYMo crystals. A $0.5Na_2MoO_4{:}0.4Na_2Mo_2O_7$ molar mixture was used as flux; the remaining 0.1 mol. of the mixture was the Yb:NaYMo solute. The solute-flux mixture was heated in a Pt crucible to 1000 °C for melting and homogenized at this temperature for 1 day. First, two crystals with nominal ≈5 at. % Yb in the melt were consecutively grown. The saturation temperature decreased from 890 °C in the first run to 869 °C for the second run as a consequence of the decrease in the solute concentration. The crystal growth started at the saturation temperature on an a-cut NaYW seed grown by the Cz method. The cooling intervals were 23 °C and 32 °C, respectively, at a rate of 0.04 °C/h. After removing the crystal from the flux, the furnace was cooled to 730 °C at 3 °C/h and later to room temperature at 15 °C/h. A third crystal with ≈10 at. % Yb in the melt was grown under similar conditions; the only essential differences were a saturation temperature of 876 °C, a cooling interval of 33 °C, and the use of a c-cut ≈5 at. % Yb:NaYMo TSSG seed. Crystals grown by the TSSG method were transparent [see Fig. 1(c)], thus they did not require annealing. The residual absorption in the visible (360–800 nm) is nearly constant and much lower than that observed in Cz-grown crystals. Moreover, the band edge itself appears at a wavelength about 10 nm shorter than in Cz-crystals (see Fig. 2).

The cationic composition of the crystals was determined by x-ray fluorescence spectrometry (XRFS) using Philips equipment, model MagiX Super Q, with a 2.4 kW Rh x-ray generator. Ground Yb:NaYMo single crystals and Na_2CO_3–Y_2O_3–Yb_2O_3–MoO_3 powder mixtures were melted in $Li_2B_4O_7$ to eliminate particle size effects. The latter were used to build individual calibration curves for Na, Y, Yb, and Mo cations. The K_α x-ray emission of Na, Y, and Mo and the $L_{\alpha 1}$ of Yb were diffracted by an LiF 200 crystal analyzer using a 150 μm collimator. Four crystals were independently analyzed, and the composition results are summarized in Table 1. First, it must be noted that the Na content in the analyzed TSSG crystal is close to

Table 1. $NaY(MoO_4)_2$ Crystals Grown by Cz and TSSG Methods[a]

Crystal Reference	Growth Method	$[Yb]_{melt}$ [at. %]	$Yb_{crystal}$ [at. %]	$[Yb]_{crystal}$ [10^{20} cm^{-3}]	Crystal Composition^{XRFS}
1	Cz	1	0.8	0.537^{XRFS}	$Na_{0.919}Y_{1.018}Yb_{0.008}(Mo_1O_4)_2$
2	Cz	10	8.7	5.70^{XRFS}	$Na_1Y_{0.932}Yb_{0.087}(Mo_1O_4)_2$
3	Cz	10	8.4	5.50^{XRFS}	$Na_{0.910}Y_{0.946}Yb_{0.084}(Mo_1O_4)_2$
4	TSSG	≈5	3.3	2.16^{XRFS}	$Na_{0.976}Y_{1.307}Yb_{0.033}(Mo_{0.986}O_4)_2$
5	TSSG	≈5	3.6	2.36^{OA}	
6	TSSG	≈10	6.1	4.03^{OA}	

[a]Crystal composition determined from XRFS. Values in italic were taken equal to the nominal composition. Ytterbium density in the melt, $[Yb]_{melt}$, and in the crystal, $[Yb]_{crystal}$. The Yb concentration of crystals with reference [5,6] was calculated from the integrated OA of Yb^{3+}.

the nominal one corresponding to the DM formula and significantly larger than in Cz-grown crystals. Further analyses of the Na content of Cz-grown crystals before and after annealing showed no significant difference. Although the molybdenum content is always very close to the nominal composition, particularly for Cz-grown crystals, the crystals grown by the TSSG method exhibit a small Mo deficiency. The Na and Mo deficiencies are compensated by extra incorporation of trivalent cations, Y and Yb. The segregation coefficient of Yb in the Cz-grown crystals is about ≈0.85. Taking into account the NaYMo cell volume ($V=305.23$ Å^3), we calculated independently the Yb density ([Yb]) in four crystals (see Table 1); [Yb] in the two remaining TSSG crystals was deduced from the comparison of the integrated OA of Yb^{3+} bands.

NaYMo is a uniaxial crystal. The ordinary n_o ($\mathbf{E}\perp\mathbf{c}$) and extraordinary n_e ($\mathbf{E}\|\mathbf{c}$) refractive indices were measured at 25 °C by the minimum deviation method using properly oriented prisms of 6.1 at. % Yb:NaYMo grown by the TSSG method. The uncertainty in these measurements is ±0.002. The crystal birefringence is small, $n_e-n_o<0.01$. Figure 3 shows measured refractive indices and the fit of the experimental data to a single-pole Sellmeier law $n^2=A+[B/1-(C/\lambda)^2]$ with the parameters included in the inset. Additional measured refractive indices for a 3.6 at. % Yb:NaYMo (TSSG) as well as those reported in [18] for a 1.66 at. % Yb:NaYMo (Cz-grown) were within the uncertainty of the data in Fig. 3. Therefore it can be concluded that the influence of Yb doping on this physical property is minor.

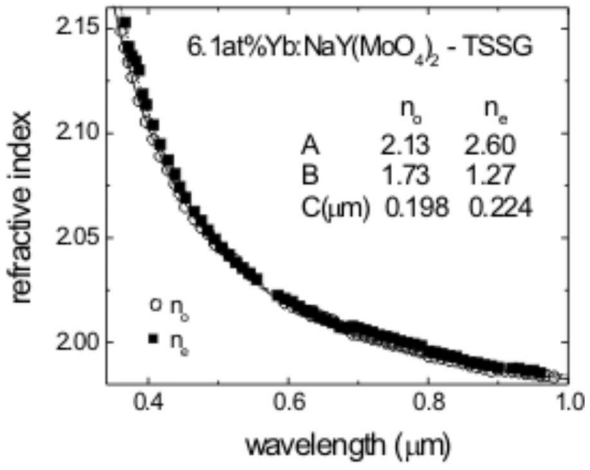

Fig. 3. Room temperature ordinary (open circles) and extraordinary (closed squares) refractive indices of a 6.1 at. % Yb:NaYMo crystal grown by the TSSG method. The solid curve (n_o) and the dashed curve (n_e) are the fits to a single-pole Sellmeier law with the parameters given in the inset.

3. Yb^{3+} OPTICAL SPECTROSCOPY

Regarding the Yb^{3+} spectroscopy no difference was found between Cz and TSSG crystals. Detailed single crystal x-ray diffraction studies of several tetragonal DT and DM crystals ($NaTW$, $T=Y$ [13] Gd [6], Lu [13], and Bi [20]) have determined the $I\bar{4}$ space group for the crystalline structure for which the existence of two independent 2*b* and 2*d* crystal sites shared by Na^+ and T^{3+} cations was demonstrated. To determine the spectroscopic contributions of Yb^{3+} in these two sites of the NaYMo host, cryogenic (6 K) optical measurements were performed. OA was measured using a Varian spectrophotometer, model CARY-5E. Photoluminescence was excited with a Ti: sapphire laser, dispersed by a SPEX 340-E ($f=34$ cm) spectrometer, and detected with a 77 K cooled Ge photodiode and a lock-in amplifier. The general features of the 6 K OA of Yb^{3+} in NaYMo are similar to those observed in other tetragonal DT and DM single crystals. Three band sets corresponding to $^2F_{7/2}(0)\rightarrow{}^2F_{5/2}(0',1',2')$ transitions are observed in the 974–976, 955–970, and 930–950 nm spectral regions, respectively. The last one is of a complex nature, and it is only seen in σ-polarization while the first two are observed in σ and π-spectra but do not show evidence of overlapped components. Figure 4(a) shows the σ-polarized OA that contains all Yb^{3+} bands.

To reveal the spectral contributions of Yb^{3+} in the 2*b* and 2*d* sites we performed site resolved photoluminescence measurements by exciting with a Ti:sapphire laser at different wavelengths within the bandwidth of each of the above mentioned OA band sets. Figure 4(b) shows the emission spectra observed when exciting at the wings of the 955–970 nm OA. These spectra are equivalent to those obtained by excitation in the wings of the 974–976 nm OA, apart from the fact that the resonant $^2F_{7/2}(0)\rightarrow{}^2F_{5/2}(0')$ emission can not be observed due to overlapping with the exciting light. In all emission spectra, four bands due to $^2F_{5/2}(0')\rightarrow{}^2F_{7/2}(0,1,2,3)$ transitions are observed, but the band positions are sensitive to the excitation wavelength, showing the emission contributions of both Yb^{3+} sites. Exciting at intermediate wavelengths shows gradual overlapping of the two emission spectra. The Yb^{3+} site contributions to the OA spectrum are resolved in the corresponding excitation spectra

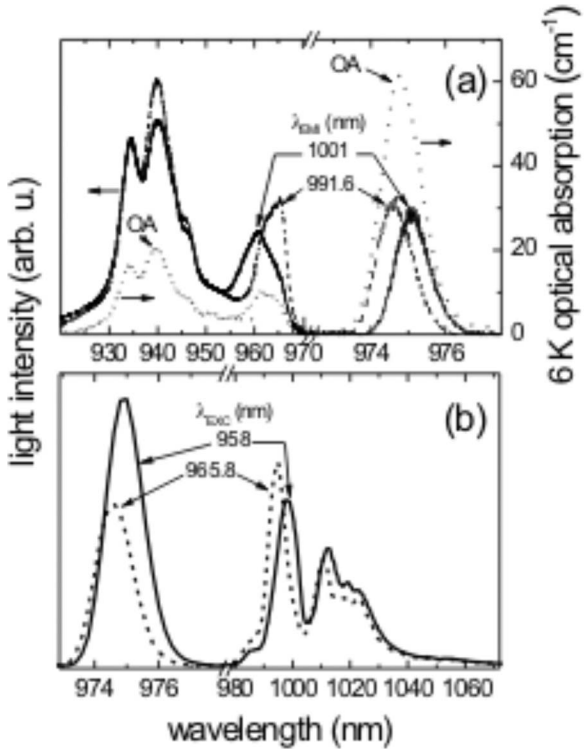

Fig. 4. (a) Comparison of the 6 K σ-polarized OA of an 8.7 at. % Yb:NaYMo sample and the excitation spectra of the 6 K unpolarized photoluminescence of a 0.8 at. % Yb:NaYMo sample detected at λ_{EMI}=991.6 and 1001 nm. (b) Unpolarized 6 K photoluminescence emission spectra of 0.8 at. % Yb:NaYMo excited at λ_{EXC}=958 and 965.8 nm.

shown in Fig. 4(a). By proper selection of the emission wavelength two well resolved peaks are determined for each of the $^2F_{7/2}(0)\rightarrow{}^2F_{5/2}(0')$ and $^2F_{7/2}(0)\rightarrow{}^2F_{5/2}(1')$ transitions while the spectral structure observed in the 930–950 nm region is not sensitive to the Yb^{3+} sites and is most likely associated with Stokes and anti-Stokes coupling of the $^2F_{5/2}(2')$ level with a $\approx$65 cm^{-1} phonon. Table 2 summarizes the $^2F_{7/2}(n)$ and $^2F_{5/2}(n')$ Stark levels determined experimentally for the two sites.

To assess the above interpretation of the site resolved photoluminescence, the obtained energy level sets were compared with those calculated using the semiempirical simple overlap crystal field model (SOM) [21] that allows one to estimate the crystal field parameters (CFPs) from the crystallographic data of the Y(or Yb)O_8 coordination polyhedra. Separate sets of CFPs for the Yb^{3+} ions in the 2*b* and 2*d* sites were derived from the corresponding Yb–O bond distances. The calculated values of the six CFPs corresponding to the S_4 symmetry were then used, independently for each site, in the simulation of the $^2F_{7/2}(n)$ and $^2F_{5/2}(n')$ Stark level energies for the $4f^{13}$ configuration. The simulation was performed using a previously developed code [22]. The used free ion parameters, the derived SOM CFPs, and the corresponding energy level schemes obtained for Yb^{3+} in each of the two sites are also included in Table 2.

Despite the presence of several Yb^{3+} centers in NaYMo in the following spectroscopic treatment it is useful to assume an average center to simplify the following calculations. For this purpose we will consider the mean values

Table 2. Free Ion (E^0 and ζ) Parameters and SOM CFPs (B_0^2, B_0^4, B_4^4, B_0^6, B_4^6, and S_4^6) Used to Calculate the $^2F_{7/2}(n)$ and $^2F_{5/2}(n')$ Energy Levels of Yb^{3+} in the 2*b* and 2*d* Sites of $NaY(MoO_4)_2$[a]

	2*d* Site	2*b* Site
E^0	4623.2	4617.0
ζ	2897.6	2900.0
B_0^2	411	492
B_0^4	−659	−622
B_4^4	±734	±699
B_0^6	−46	−23
B_4^6	±586	±554
S_4^6	±65	±129
$^2F_{5/2}(2')$	10621 (10638)	10634 (10638)
$^2F_{5/2}(1')$	10387 (10408)	10364 (10361)
$^2F_{5/2}(0')$	10255 (10255)	10261 (10261)
$^2F_{7/2}(3)$	477 (483)	491 (488)
$^2F_{7/2}(2)$	367 (378)	349 (367)
$^2F_{7/2}(1)$	254 (248)	220 (207)
$^2F_{7/2}(0)$	0 (0)	0 (0)

[a]The experimentally determined energy levels are in parentheses. All energies are relative to the $^2F_{7/2}(0)$ level for the corresponding site. Parameters and energies are given in cm^{-1}. Overlap between Yb-oxygen orbital wave functions and effective charge for oxygen are taken as 0.07 and −1.0, respectively.

of energy position of both sites, i.e., $^2F_{7/2}$ (0, 228, 372, and 485 cm^{-1}) and $^2F_{5/2}$ (10258, 10385, and 10638 cm^{-1}). This provides the partition functions of the lower and upper multiplets as Z_l=1.630 and Z_u=1.705, respectively, and Z_l/Z_u=0.956.

Figure 5 shows the absorption cross sections of Yb:NaYMo. It is worth noting that these values have been calculated independently in the four samples (1–4) of Table 1 analyzed by XRFS. The results were constant within an uncertainty of approximately ±10%. The maximum absorption cross sections at 975 nm are $2.05(\pm0.20)\times10^{-20}$ cm^2 and $3.05(\pm0.28)\times10^{-20}$ cm^2 for σ- and π-polarizations, respectively. These values are slightly lower than those previously reported for Yb:NaYMo [15] but still significantly larger than those obtained for Yb in the isostructural DT hosts [1]. The emission cross sections that are also included in Fig. 5 were calculated by the reciprocity method [23] using the Yb^{3+} energy level scheme derived from 6 K spectroscopy. Their spectral shape matches well with the Yb^{3+} photoluminescence as indicated by the symbols (open circles) in Fig. 5. These emission cross sections are the largest known for crystals of that type. The associated gain cross sections shown in Fig. 6 are also significantly larger than those of Yb:NaLaMo [14]. The expected laser wavelength in dependence on the inversion ratio β can also be estimated from Fig. 6, where β represents the ratio of the Yb^{3+} ions in the excited state to the total Yb^{3+} ion density. The $^2F_{5/2}$ radiative lifetime can be obtained by the Füchtbauer–Ladenburg method, $\tau_{rad}=(1/8\pi n^2 c)[\int(\langle\sigma_{EMI}(\lambda)\rangle/\lambda^4)d\lambda]^{-1}$, where the average is over the polarization. Taking the extrapolation of the refractive index data to 1025 nm (Fig. 3) into account, i.e., assuming an average value of $n\approx1.982$, one arrives at

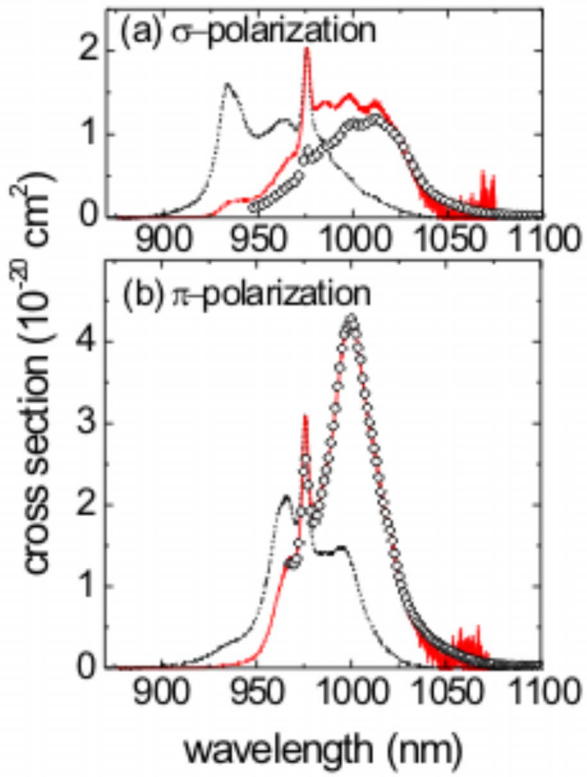

Fig. 5. (Color online) Room temperature Yb:NaYMo absorption σ_{abs} (black dashed curves) and emission σ_{em} (solid curves) cross sections for (a) σ-polarization and (b) π-polarization. The symbols (open circles) in (a) and (b) represent the photoluminescence given for comparison with the emission cross sections.

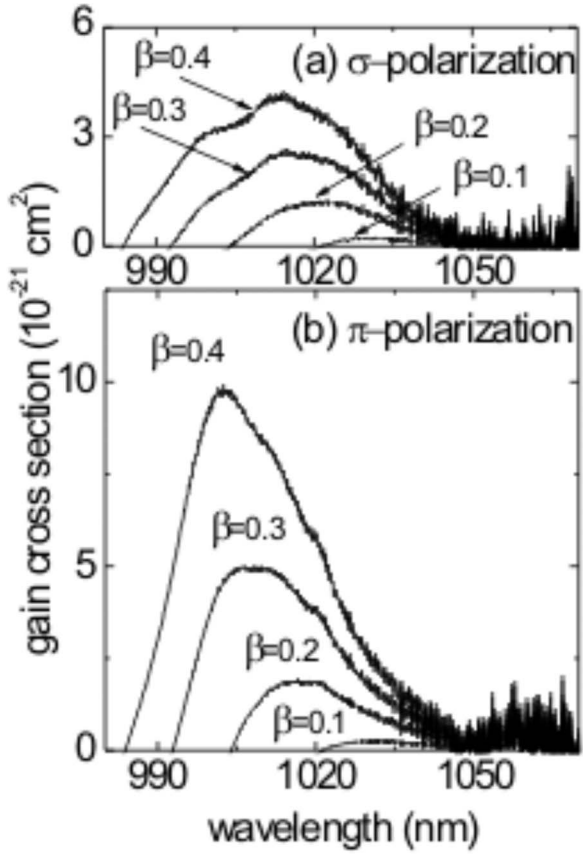

Fig. 6. Room temperature gain cross sections of Yb:NaYMo, $\sigma_{gain}=\beta\sigma_{em}-(1-\beta)\,\sigma_{abs}$, for different inversion rates β and for (a) σ-polarization and (b) π-polarization.

$\tau_{rad}=267\ \mu$s. The $^2F_{5/2}$ fluorescence lifetime was measured by the pinhole method using an 8.7 at. % Yb:NaYMo Cz-grown plate with a thickness of 220 μm. The obtained value, 290(±7) μs, is very close to the above calculated radiative lifetime but significantly shorter than the experimental value for the fluorescence decay time (535 μs) reported previously without special caution to suppress the radiation trapping effect [15].

4. LASER RESULTS

A. Continuous-Wave Laser Operation

Yb:NaYMo crystals grown by the Cz method and annealed to recover sample transparency showed rather high laser thresholds and low laser efficiencies. Therefore, they have not been studied systematically as laser media. The results presented hereafter refer exclusively to crystals grown by the TSSG method.

Continuous-wave laser operation was studied at room temperature in a standard astigmatically compensated four mirror (Z-shaped) cavity with a length of 153 cm. The uncoated samples were positioned between two concave folding mirrors of −10 cm radius of curvature (ROC) [see Fig. 7(a)]. No special provision was made for cooling the samples. A Ti:sapphire laser pump source was applied up to incident powers of 1.6 W at the absorption peak near 968 nm. The 50 μm broad-stripe InGaAs single emitter used for diode pumping with incident power up to 1.7 W had a linewidth of 4 nm (FWHM) centered at 965 nm when its temperature was adjusted to 32 °C. Its astigmatic emission was collimated by two crossed cylindrical microlenses. Its polarization degree was 0.8. In both cases the pump radiation was focused by an $f=6.28$ cm spherical lens through one of the folding mirrors. The Ti:sapphire laser pump spot had a Gaussian waist of 22 μm fitting well with the parameters of the resonator, whereas the pump waist of the diode laser amounted to 32 μm. Plane output couplers with transmission $T=1\%$, 3%, 5%, and 10% were used.

At first we studied a 3.2 mm thick 3.6 at. % Yb:NaYMo crystal under Ti:sapphire laser pumping. This a-cut sample allowed us to study both π- and σ-polarizations, and the pump polarization applied was always in the same plane. Figure 8 shows the change of the actual absorption with the incident pump power. The absorption measured without lasing is strongly bleached with increasing incident pump power in contrast to the absorption when the laser operates. This is due to the recycling effect caused by the circulating intracavity laser intensity that tends to restore the small signal absorption value. At maximum incident pump power, the Yb^{3+} absorption was bleached only slightly down to ≈75% for the π- and down to ≈65% for the σ-polarizations. The actual crystal absorption depended only somewhat on the output coupling. Continuous-wave laser operation was obtained both for σ- and π-polarizations, whereas the laser thresholds and slope efficiencies were similar as shown in Fig. 9. Both the laser wavelength (λ) and the slope efficiency (η) with re-

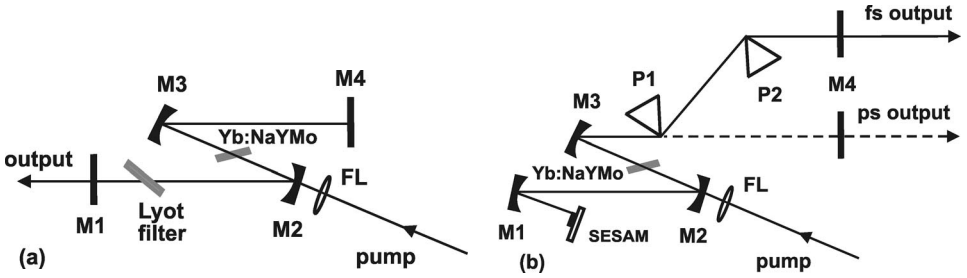

Fig. 7. Optical cavities used to study the laser performance of Yb:NaYMo. M2 and M3, folding mirrors; FL, focusing lens. (a) cw operation. M1, output coupler; Lyot filter, frequency selecting element; M4, plane total reflector. (b) Mode-locked operation. SESAM, semiconductor saturable absorber mirror; M1, focusing mirror; P1 and P2, LaFN28 Brewster prisms; M4, output coupler.

spect to the absorbed power are indicated in Figs. 9(a) and 9(b). For the π-polarization [Fig. 9(a)], a maximum output power of 480 mW was achieved at $\approx$1028 nm by using $T=5\%$. In this case, the laser threshold and the slope efficiency were 200 mW (absorbed pump power) and 63%, respectively. Due to the lower absorption for the σ-polarization the maximum output power was limited to 360 mW applying $T=3\%$ [Fig. 9(b)]. The maximum slope efficiency of 63% with $T=10\%$ was the same as with π-polarization. The somewhat higher gain cross section of the π-polarization (Fig. 6) has little effect on the output power results, whereas the increase of the emission wavelength for smaller values of the output coupling is more pronounced for the π-polarization as can be expected from Fig. 6. The slope efficiencies achieved with Ti:sapphire laser pumping are roughly two times higher than with Yb:NaLaMo using a similar setup [11], and exceed slightly the values for Yb:LiGdMo obtained with a more compact cavity [9].

The cw laser tunability was studied with a two-plate birefringent filter in the cavity arm containing the output coupler [see Fig. 7(a)]. The tunability was measured using a 1.73 mm thick 3.3 at. % Yb:NaYMo sample oriented for π-polarization. Figure 10 shows the results obtained for two output couplers. The continuous tuning range extended from 1005 to 1059 nm for 1% output coupling with a FWHM of 40 nm.

Diode laser pumping of the same crystal as used for the tunable operation was only studied for π-polarization. The results are shown in Fig. 11. The maximum incident

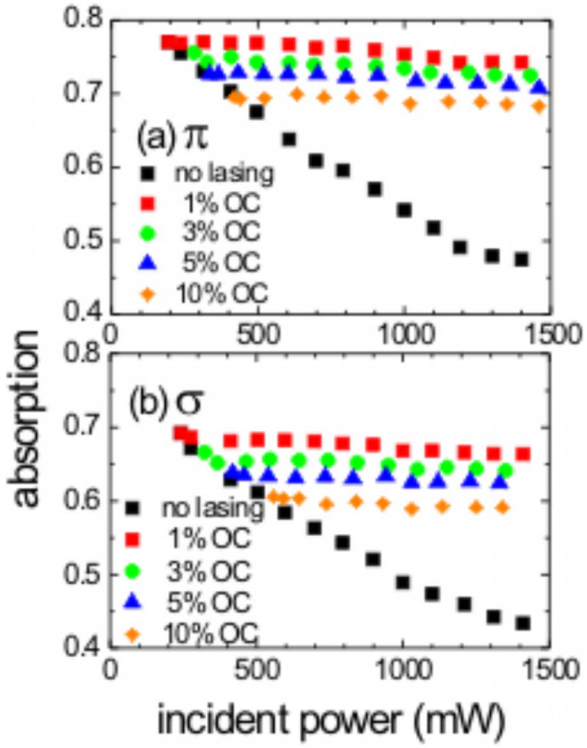

Fig. 8. (Color online) Single-pass absorption versus incident pump power of the 3.2 mm thick 3.6 at. % Yb:NaYMo crystal for (a) π-polarization and (b) σ-polarization, measured without lasing and under laser operation for the used output couplers.

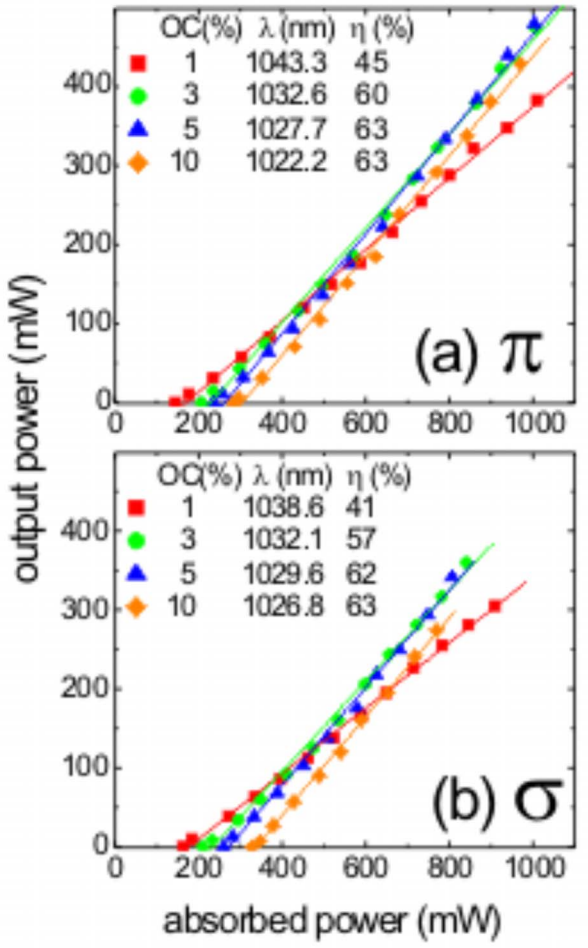

Fig. 9. (Color online) Continuous-wave laser performance of the 3.2 mm thick 3.6 at. % Yb:NaYMo crystal with Ti:sapphire laser pumping for (a) π-polarization and (b) σ-polarization (OC, output coupler transmission; λ, laser wavelength; η, slope efficiency).

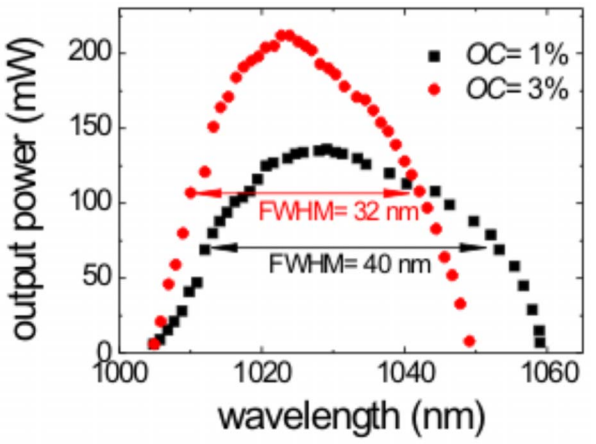

Fig. 10. (Color online) Laser tuning of the 1.73 mm thick 3.3 at. % Yb:NaYMo crystal in π-polarization with Ti:sapphire laser pumping for two output coupler transmissions (OC).

pump power on the crystal was limited to 1.5 W. The maximum output power achieved with the diode pumped Yb:NaYMo laser was 175 mW corresponding to an absorbed pump power of 750 mW. In terms of absorbed pump power the maximum slope efficiency amounted to 38.6% for the 5% output coupler. The laser wavelength was 1021.6 nm and got longer for decreasing transmission of the output coupler as in the case of Ti:sapphire laser pumping. The lowest laser threshold achieved was 165 mW for a 1% output coupler. The measured absorption amounted to ~50%, less in comparison to Ti:sapphire laser pumping due to the lower thickness and doping level of the sample used. The achieved slope efficiencies with diode pumping are also relatively high, keeping in mind that they were obtained with the same cavity configuration.

B. Mode-Locked Operation

The cavity setup is illustrated in Fig. 7(b). The experiments were performed only with the Ti:sapphire laser as a pump source. We studied longitudinal pumping in a Z-shaped astigmatically compensated resonator with two folding mirrors (ROC=−10 cm) in the middle to form a 30 μm cavity waist at the position of the Yb:NaYMo crystal. The 1.73 mm thick TSSG grown 3.3 at. % Yb:NaYMo sample oriented for π-polarization, as investigated for the cw tuning experiments, was used. The crystal was mounted under a Brewster angle between the two folding mirrors. One arm of the resonator contained an additional focusing mirror (ROC=−15 cm) to increase the intensity on the semiconductor saturable absorber mirror (SESAM) that terminated the resonator. The other arm contained a plane output coupler and two dispersion compensating prisms could be inserted. The SESAM was grown by the metal-organic chemical-vapor deposition (MOCVD) method and consisted of a bottom Bragg mirror comprising 25 pairs AlAs/GaAs quarter wave layers designed for a central wavelength of 1030 nm. The reflection band extended from 980 to 1070 nm. The absorber was a 10 nm thick InGaAs surface quantum well structure [24] with a saturable absorption of ≈1%. Its relaxation time was measured by the pump-probe technique to be less than 5 ps.

When the cavity for mode locking was used without intracavity prisms [Fig. 7(b)], the laser operated in the picosecond regime with a pulse repetition rate of 94 MHz. Pulses as short as 1.74 ps near 1020 nm were obtained at a maximum output power of 193 mW with a 3% output coupler. The measured autocorrelation traces were fitted assuming a sech^2-pulse shape. In Fig. 12(a) a typical autocorrelation function is shown together with the emission spectrum. The 8.4 nm broad spectrum (FWHM) could support pulses of sub-150 fs duration, which means that the generated pulses are strongly chirped and the pulse duration in the picosecond mode exceeds the Fourier limit by a factor of about 10 [Fig. 12(a), inset].

For femtosecond operation, we optimized first the cavity design in order to obtain the shortest pulse duration. To this aim, two LaFN28 Brewster prisms with a tip-to-tip separation of 45 cm were inserted into the arm containing the output coupler [Fig. 7(b)]. The resulting pulse repetition rate was 90 MHz. The deconvolved FWHM of the shortest pulse was 91 fs for an average power of 20 mW when using the 1% output coupler. The corresponding output spectrum was centered at 1026 nm and had a bandwidth of 12.9 nm. This results in a time-bandwidth product of 0.33 corresponding to nearly transform-limited sech^2-pulses. The intensity autocorrelation trace together with the corresponding fit and the spectrum of the shortest pulses are shown in Fig. 12(b). Both experimental data (squares) and the fit (curve) are plotted. Using T=5% the output power could be increased to 125 mW with only slightly longer pulse durations of 117 fs. The results obtained with the first mode-locked Yb-doped DM crystal, with pulse durations in the sub-100 fs range, make us optimistic for reaching shorter pulses after optimization of the Yb-concentration and growth conditions. The achieved pulse duration of the Yb:NaYMo laser in the femtosecond regime is comparable to the results obtained with its Yb-doped DT "counterparts" NaLuW [8] and NaGdW [6]. Shorter pulse durations (53 fs) were obtained only based on Yb:NaYW as mentioned in section 1 [1].

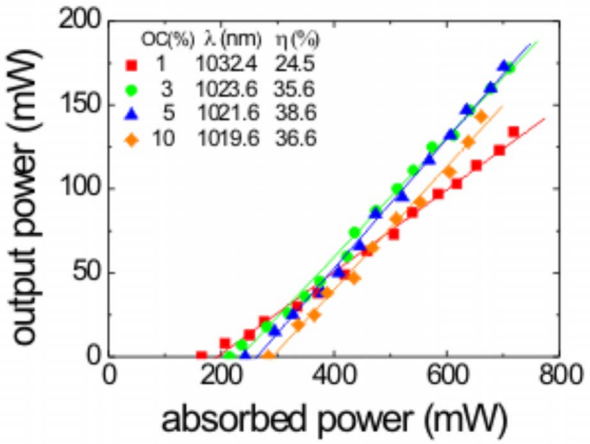

Fig. 11. (Color online) Continuous-wave laser performance of the 1.73 mm thick 3.3 at. % Yb:NaYMo sample in π-polarization with diode laser pumping (OC, output coupler transmission; λ, laser wavelength; η, slope efficiency).

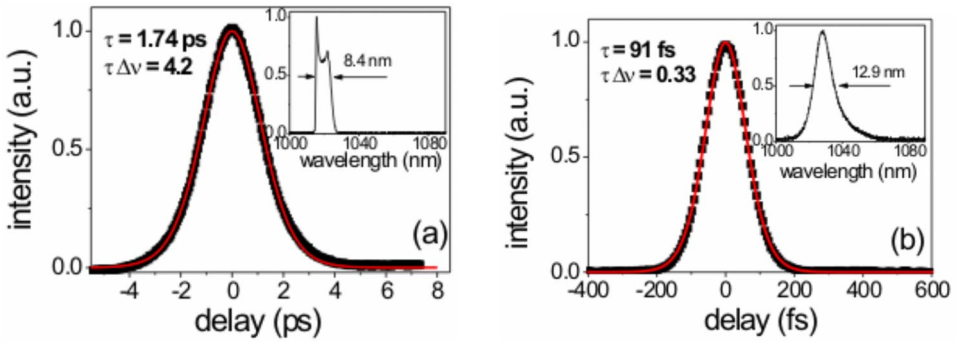

Fig. 12. (Color online) Autocorrelation traces (symbols denote the measurements and curves denote the fits) and spectra (insets) of the Yb:NaYMo laser in the (a) picosecond and (b) femtosecond regime (τ, pulse duration; $\tau\Delta\upsilon$, time-bandwidth product).

5. CONCLUSIONS

Yb-doped $NaY(MoO_4)_2$ single crystals have the largest absorption and emission cross sections so far observed in a tetragonal DT or DM crystal. Moreover, they possess broad optical bandwidths induced by the presence of several Yb^{3+} centers, namely, the 2*b* and 2*d* crystal sites, each one with several lattice environments. Evidence of these centers has been supplied by low temperature (6 K) site resolved optical spectroscopy, and the energy levels corresponding to Yb^{3+} in each site have been assessed by crystal field modeling.

$NaY(MoO_4)_2$ crystals can be grown either directly from their congruent melt using the Cz growth method or using a melted flux by the TSSG method. The first method requires heating to a high temperature ($\approx$1160 °C), and the crystals grown appear colored due to an electronic reduction process. Although crystal transparency can be partially recovered by oxidation annealing in air at 900 °C, the remaining point defects act as killing centers for the Yb^{3+} photoluminescence leading to high laser thresholds and low laser slope efficiencies. Crystals grown by the TSSG method in an $x Na_2MoO_4$:$y Na_2Mo_2O_7$ flux require lower growth temperatures (<890 °C) and are fully transparent down to $\approx$360 nm. These crystals are positive uniaxial with rather small birefringence $\Delta n \approx 0.01$.

Continuous-wave laser operation of TSSG grown $NaY(MoO_4)_2$ has been demonstrated for 3.3 and 3.6 at % Yb^{3+} doping with Ti:sapphire laser and diode laser pumping. Using a 3.2 mm thick 3.6 at. % Yb:$NaY(MoO_4)_2$ sample and π-polarization, the maximum slope efficiency reached was 63% and the maximum output power was 480 mW for an absorbed pump power of 1 W. The pump thresholds (absorbed power) were around 200 mW, depending on the output coupler. The Yb:$NaY(MoO_4)_2$ laser was continuously tunable over 54 nm at zero level, centered near 1028 nm. Passive mode locking of a Yb-doped DM was demonstrated for the first time to our knowledge. Using a SESAM, pulses as short as 91 fs at a wavelength of 1026 nm were achieved.

ACKNOWLEDGMENTS

This work was supported by the project MAT2005-6354-C03-01 (Spain). X. Han, J. M. Cano-Torres, and A. García-Cortés were supported by the Spanish Science and Education Ministry through Juan de la Cierva, I3P-BPD2005 and research training grants. The experimental contributions of C. Kränkel and K. Petermann (Hamburg University) in lifetime measurements and those of F. J. Valle [Consejo Superior de Investigaciones Cientificas (CSIC)] in the measurement of the Yb concentration are also acknowledged.

REFERENCES

1. A. García-Cortés, J. M. Cano-Torres, M. D. Serrano, C. Cascales, C. Zaldo, S. Rivier, X. Mateos, U. Griebner, and V. Petrov, "Spectroscopy and lasing of Yb-doped $NaY(WO_4)_2$: Tunable and femtosecond mode-locked laser operation," IEEE J. Quantum Electron. **43**, 758–764 (2007).
2. J. Liu, H. Zhang, J. Wang, and V. Petrov, "Continuous-wave and *Q*-switched laser operation of Yb:$NaY(WO_4)_2$ crystals," Opt. Express **15**, 12900–12904 (2007).
3. G. Q. Xie, D. Y. Tang, H. J. Zhang, J. Y. Wang, and L. J. Qian, "Efficient operation of a diode-pumped Yb:$NaY(WO_4)_2$ laser," Opt. Express **16**, 1686–1691 (2008).
4. J. Liu, J. M. Cano-Torres, C. Cascales, F. Esteban-Betegón, M. D. Serrano, V. Volkov, C. Zaldo, M. Rico, U. Griebner, and V. Petrov, "Growth and continuous-wave laser operation of disordered crystals of Yb^{3+}:$NaLa(WO_4)_2$, Yb^{3+}:$NaLa(MoO_4)_2$," Phys. Status Solidi A **202**, R29–R31 (2005).
5. J. Liu, J. M. Cano-Torres, F. Esteban-Betegón, M. D. Serrano, C. Cascales, C. Zaldo, M. Rico, U. Griebner, and V. Petrov, "Continuous-wave diode-pumped operation of an Yb:$NaLa(WO_4)_2$ laser at room temperature," Opt. Laser Technol. **39**, 558–561 (2007).
6. C. Cascales, M. D. Serrano, F. Esteban-Betegón, C. Zaldo, R. Peters, K. Petermann, G. Huber, L. Ackermann, D. Rytz, C. Dupré, M. Rico, J. Liu, U. Griebner, and V. Petrov, "Structural, spectroscopic and tunable laser properties of Yb^{3+}-doped $NaGd(WO_4)_2$," Phys. Rev. B **74**, 174114 (2006).
7. J. Liu, V. Petrov, H. Zhang, J. Wang, and M. Jiang, "Efficient passively *Q*-switched laser operation of Yb in the disordered $NaGd(WO_4)_2$ crystal host," Opt. Lett. **32**, 1728–1730 (2007).
8. A. García-Cortés, J. M. Cano-Torres, X. Han, C. Cascales, C. Zaldo, X. Mateos, S. Rivier, U. Griebner, V. Petrov, and F. J. Valle, "Tunable continuous wave and femtosecond mode-locked Yb^{3+} laser operation in $NaLu(WO_4)_2$," J. Appl. Phys. **101**, 063110 (2007).
9. M. Rico, U. Griebner, V. Petrov, P. Ortega, X. Han, C. Cascales, and C. Zaldo, "Growth, spectroscopy, and tunable laser operation of the disordered crystal $LiGd(MoO_4)_2$ doped with ytterbium," J. Opt. Soc. Am. B **23**, 1083–1090 (2006).
10. A. V. Mandrik, A. E. Troshin, V. E. Kisel, A. S. Yasukevich, G. N. Klavsut, N. V. Kuleshov, and A. A. Pavlyuk, "CW and

Q-switched diode-pumped laser operation of Yb^{3+}:$NaLa(MoO_4)_2$," Appl. Phys. B **81**, 1119–1121 (2005).
11. M. Rico, J. Liu, J. M. Cano-Torres, A. García-Cortés, C. Cascales, C. Zaldo, U. Griebner, and V. Petrov, "Continuous wave and tunable laser operation of Yb^{3+} in disordered $NaLa(MoO_4)_2$," Appl. Phys. B **81**, 621–625 (2005).
12. R. Peters, C. Kränkel, K. Petermann, and G. Huber, "Power scaling potential of Yb:NGW in thin disk laser configuration," Appl. Phys. B **91**, 25–28 (2008).
13. X. Han, A. García-Cortés, M. D. Serrano, C. Zaldo, and C. Cascales, "Structural and thermal properties of tetragonal double tungstate crystals intended for ytterbium laser composites," Chem. Mater. **19**, 3002–3010 (2007).
14. Yu. K. Voron'ko, K. A. Subbotin, V. E. Shukshin, D. A. Lis, S. N. Ushakov, A. V. Popov, and E. V. Zharikov, "Growth and spectroscopic investigations of Yb^{3+}-doped $NaGd(MoO_4)_2$ and $NaLa(MoO_4)_2$—new promising laser crystals," Opt. Mater. **29**, 246–252 (2006).
15. X. Li, Z. Lin, L. Zhang, and G. Wang, "Growth and spectral properties of Yb^{3+}-doped $NaY(MoO_4)_2$ crystal," Opt. Mater. **29**, 728–731 (2007).
16. X. Lu, Z. You, J. Li, Z. Zhu, G. Jia, B. Wu, and C. Tu, "Spectroscopic analysis of Ho^{3+} in a $NaY(MoO_4)_2$ single crystal," J. Phys. D: Appl. Phys. **39**, 3755–3759 (2006).
17. X. Lu, Z. You, J. Li, Z. Zhu, G. Jia, B. Wu, and C. Tu, "The optical properties of Dy^{3+}-doped $NaY(MoO_4)_2$ crystal," J. Lumin. **126**, 63–67 (2007).
18. X. Lu, Z. You, J. Li, Z. Zhu, G. Jia, B. Wu, and C. Tu, "Thermal, optical and spectroscopic assessment of Yb^{3+}:$NaY(MoO_4)_2$ single crystal as a potential diode pumped laser near 1.04 μm," Solid State Commun. **146**, 287–292 (2008).
19. M. D. Serrano, F. Esteban-Betegón, and C. Zaldo, "Growth and spectroscopic investigation of ytterbium-doped $NaLa(WO_4)_2$ single crystals," J. Cryst. Growth **275**, e819–e825 (2005).
20. M. Rico, A. Méndez-Blas, V. Volkov, M. Á. Monge, C. Cascales, C. Zaldo, A. Kling, and M. T. Fernández-Díaz, "Polarization and local disorder effects on the properties of Er^{3+}-doped $XBi(YO_4)_2$, X=Li or Na and Y=W or Mo, crystalline tunable laser hosts," J. Opt. Soc. Am. B **23**, 2066–2078 (2006).
21. P. Porcher, M. Couto dos Santos, and O. Malta, "Relationship between phenomenological crystal field parameters and the crystal structure: The simple overlap model," Phys. Chem. Chem. Phys. **1**, 397–405 (1999).
22. A. Méndez-Blas, M. Rico, V. Volkov, C. Cascales, C. Zaldo, C. Coya, A. Kling, and L. C. Alves, "Optical spectroscopy of Pr^{3+} in $M^+Bi(XO_4)_2$, M^+=Li or Na and X=W or Mo, locally disordered single crystals," J. Phys. Condens. Matter **16**, 2139–2160 (2004).
23. D. E. McCumber, "Einstein relations connecting broadband emission and absorption spectra," Phys. Rev. **136**, A954–A957 (1964).
24. F. Saas, G. Steinmeyer, U. Griebner, M. Zorn, and M. Weyers, "Exciton resonance tuning for the generation of sub-picosecond pulses from a mode-locked semiconductor disk laser," Appl. Phys. Lett. **89**, 141107 (2006).